Peer-reviewed version available at *Algorithms* **2020**, *13*, 24; doi:10.3390/a13010024

Article

Unstructured uncertainty based modeling and robust stability analysis of textile-reinforced composites with embedded shape memory alloys

Najmeh Keshtkar [1,*], **Klaus Röbenack** [1]

[1] Institute of Control Theory, Technische Universität Dresden, 01062 Dresden, Germany; {najmeh.keshtkar, klaus.roebenack}@tu-dresden.de

* Correspondence: najmeh.keshtkar@tu-dresden.de;

Abstract: This paper develops the mathematical modeling and deflection control of a textile-reinforced composite integrated with shape memory actuators. The model of the system is derived using identification method and unstructured uncertainty approach. Based on this model and robust stability analysis a robust proportional-integral controller is designed for controlling the deflection of the composite. The performance of the proposed controller is compared with a classical one through experimental analysis.

Keywords: Textile reinforced composite; Shape memory alloy; Robust stability

1. Introduction

Soft robots have been used in a wide range of applications with a projected growth of use in the following years [1,2]. The growing interest in soft robots comes from the good performance of these materials in environments which is not best suited for conventional rigid bodies. Soft robots utilize the compliance, adaptability and flexibility of soft materials and actuation methods to develop highly adaptive structures [3]. Soft robots are composed primarily of materials with low Young's modulus (around 1 GPa) which includes materials such as silicone, rubber, or other elastomeric polymers. The strength and stiffness of these soft materials can be improved by adding reinforcement materials such as fibers. The resulting combination called textile reinforced composites is lightweight, strong and resistant which makes it ideal for diverse soft robotics applications [4].

The elastic properties of textile reinforced composites require smart actuators which possess adaptability and deformability. Smart materials such as piezoelectric materials, shape memory alloys (SMA) and dielectric elastomers have been used in diverse flexible structures [5–7]. Among these smart materials, SMAs have the advantages of simple structure, small size, excellent (i.e., higher) force to weight ratio, large displacement and high stiffness [8–10]. SMAs are capable of returning to a predefined shape when heated [11]. This phenomenon is called the Shape Memory Effect (SME) and is due to crystalline phase transformation from martensite (low temperature phase) to austenite (high temperature phase) [12]. This transformation gives rise to a hysteresis effect which is highly nonlinear. While contracted upon heating, the SMAs exerts a force which is used for actuation. One of the efficient methods for heating the SMAs is resistive heating from an electrical current. Through this method, the deflection and retraction of the wire can be made controllable.

The efficiency of a shape memory actuator depends on the accuracy of its controls, which in turn depends on the mathematical model of the SMA. Among the different modelling approaches available in the literature, phenomenological or macro approaches are more suitable to be used for engineering applications. This includes constitutive models like the Tanaka model [13], the Liang and

Peer-reviewed version available at Algorithms 2020, 13, 24; doi:10.3390/a13010024

Rogers model [14], the Brinson model [15], and the hysteresis models such as the Preisach model [16], the Krasnosel'skii–Pokrovskii model [17], and the Prandtl–Ishlinskii model [18]. However, due to the complicated dynamics of the hysteresis effect in SMAs, these models are mainly complex and difficult to use for designing a suitable controller. Furthermore, not only the modelling of the involved SMA actuators is required, but of the structure of the entire system as well. One alternative for obtaining the mathematical model of the system is using experimental modelling or system identification to derive simpler equations [19,20]. The nonlinear relationship between the inputs and outputs of the system can be then represented by a linear transfer function which includes the nonlinearities of the system as unstructured uncertainty.

The purpose of this paper is to use the unstructured uncertainty approach for modelling a textile-reinforced composite system actuated by shape memory alloys. The paper extends preliminary findings presented in the conference paper [21]. Different uncertainty models are introduced, applied to the system and consequently compared. A proportional-integral controller based on the robust stability analysis is then designed to verify the effectiveness of this approach. The objective of the controller is to stabilize the position of the system for a fixed reference. The performance of this controller is compared with a classical one.

The rest of the paper is organized as follows. In Section 2 we describe the test bench. The system identification is addressed in Section 3. We carry out classical controller design in Section 4. The main contribution is the design of a robust controller discussed in Section 5. Finally, we will draw some conclusions in Section 6.

2. System Description

Figure 1 shows the experimental platform of the textile-reinforced composite with integrated SMA actuators [22]. It consists of a textile composite made from a fabric as reinforcement, covered with silicone rubber matrix.

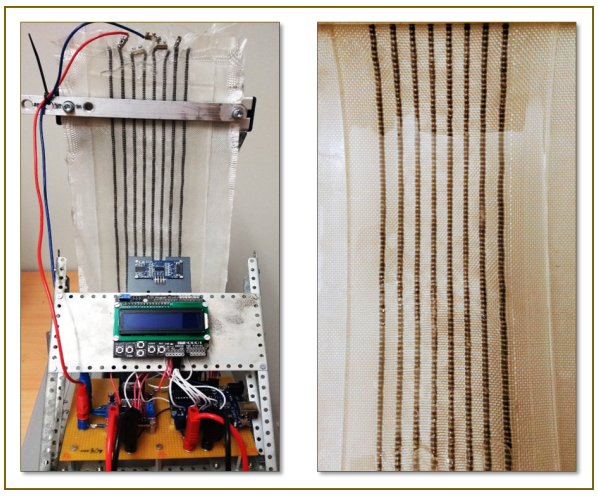

Figure 1. Textile-reinforced composite with integrated SMAs

In the composite, the SMAs are placed close to the top surface so that a phase transition of the SMA wires will bend the composite as shown in Fig. 2 . When thermally activated, the SMA actuators contract and cause a mechanical tension inside the composite. The SMA thermal stimulus is acquired by applying a voltage, which in turn causes a current flow through the wires.

The voltage to heat the SMAs is provided by a 30 V DC power supply and controlled by an L298N driver IC [23] via pulse width modulation (PWM). To measure the deflection of the textile composite we employed a Sharp GP2Y0A41SK0F distance sensor [24,25]. The control algorithms are implemented on an Arduino Uno board [25]. More details on the experimental setup are presented in [21,22].

Peer-reviewed version available at Algorithms 2020, 13, 24; doi:10.3390/a13010024

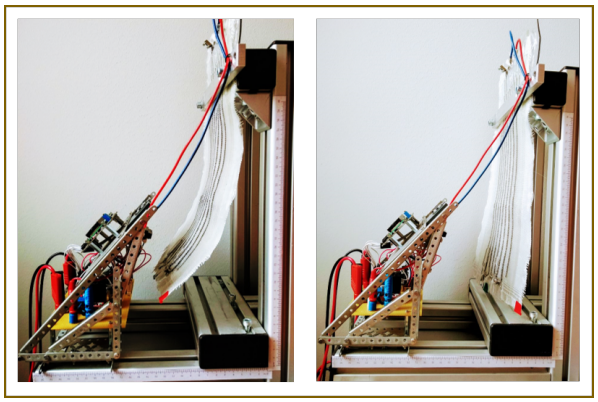

Figure 2. Deflection of the textile reinforced composite actuated by shape memory alloys

3. Model Identification

One of the main limitations of the SMA actuators is the difficulties in motion control due to hysteresis and nonlinearities. The reason that gives rise to hysteresis is that the material's crystalline structure shifts between martensite and austenite phases depending on the applied temperature and stress. Martensite, is the relatively soft and easily deformed phase of shape memory alloys, which exists at lower temperatures whereas the austenite phase is relatively hard and occurs at higher temperatures. The hysteresis of the shape memory actuators of the experimental platform for four consecutive heating up- cooling down cycles is shown in Fig. 3.

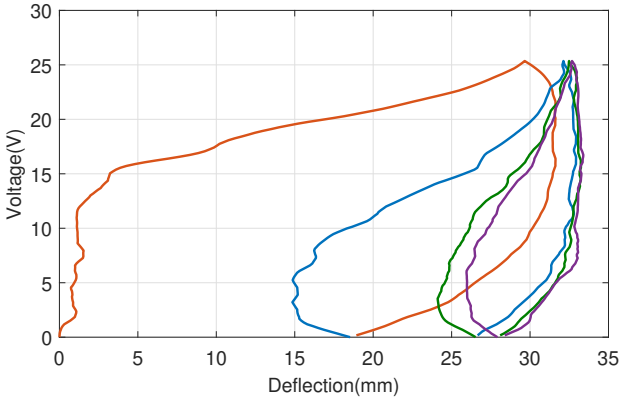

Figure 3. Hysteresis of shape memory alloy for four consecutive heating up- cooling down cycles

The system responds with a time lag to the applied voltage. In addition, there is almost no overshoot. For these reasons, we want to describe the system's essential behaviour by the first order transfer function

$$G(s) = \frac{K}{1+sT} \tag{1}$$

with gain $K > 0$ and time constant $T > 0$. The SMA wire actuator is then tested with different step inputs to obtain an interval of K and T, in which the system operates:

$$K \in [\underline{K}, \overline{K}] \quad \text{and} \quad T \in [\underline{T}, \overline{T}]. \tag{2}$$

This interval model is later extended to a dynamic uncertainty model in order to capture the hysteresis and other unmodelled dynamics.

For the identification, the System Identification Toolbox™ of MATLAB® is used [26]. This toolbox provides an efficient way for creating different mathematical models of systems such as continuous-time and discrete-time transfer functions, process models, and state space models. To

Peer-reviewed version available at Algorithms 2020, 13, 24; doi:10.3390/a13010024

describe the characteristics of the SMA actuator over a wide range of operationg points, open-loop tests of the actuator using step inputs are conducted. The input and output values of these experiments are used to identify the mathematical model (1) of the system. Each step response yields different values of the parameters K and T. Over all experiments we obtained the following upper and lower bounds of these parameters [21]:

$$\underline{K} = 1.969, \quad \overline{K} = 2.6328, \quad \underline{T} = 112.676, \quad \overline{T} = 382.995. \tag{3}$$

Subsequently, a nominal transfer function

$$\widetilde{G}(s) = \frac{\widetilde{K}}{1 + s\widetilde{T}} \tag{4}$$

of the plant can be derived using the mean values of the K and T intervals with the (nominal) parameter values $\widetilde{K} \approx 2.3009$ and $\widetilde{T} \approx 247.8355$.

4. Classical Controller Design

To control the position of the textile reinforced composite, a simple proportional integral (PI) controller is used [27,28]. Let e be the error between the desired position and the output y which is the plant measured deflection, Fig. 4. Then, the overall control function can be expressed by

$$u(t) = K_p e(t) + \int_0^t e(\tau)\,\mathrm{d}\,\tau \tag{5}$$

The controller's output signal u is the averaged voltage imposed into the system by PWM (see Section 2). In the frequency domain, this controller can be described by the transfer function

$$C(s) = \frac{U(s)}{E(s)} = K_p + \frac{K_i}{s} \tag{6}$$

with the coefficients K_p and K_i for the proportional and integral action, respectively.

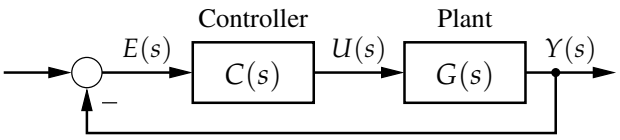

Figure 4. Simplified structure of the closed control loop

The transfer function of the (nominal) closed loop system using the plant equation (4) can be expressed as follows

$$\frac{Y(s)}{U(s)} = \frac{\widetilde{K}K_p s + \widetilde{K}K_i}{\widetilde{T}s^2 + (\widetilde{K}K_p + 1)s + \widetilde{K}K_i}. \tag{7}$$

The range of the proportional and integral gains for which the characteristic polynomial of the closed loop system is stable is given by

$$K_i > 0, \quad K_p > -\widetilde{K}.$$

For practical reasons, we will use $K_p > 0$. Based on Ziegler–Nichols tuning method [29], the gain values $K_p = 3$ and $K_i = 1.1$ are obtained for the controller. The controlled deflection of the system for a reference of 22 mm is shown Fig. 5.

Peer-reviewed version available at Algorithms 2020, 13, 24; doi:10.3390/a13010024

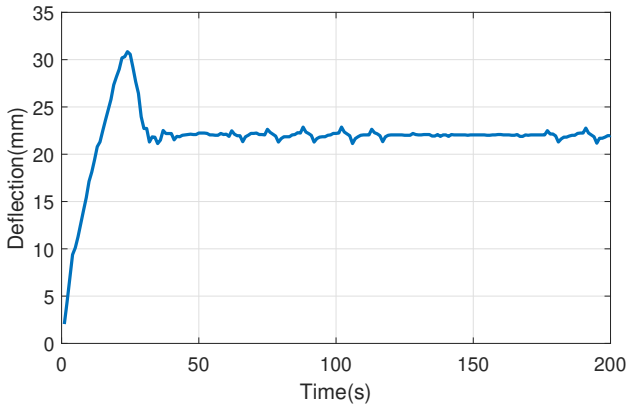

Figure 5. Controlled deflection of the system for a reference of 22 mm using classical PI controller

5. Robust Control

5.1. Uncertainty Models

When the exact model of a physical system is not known due to for example unmodelled dynamics or nonlinearities, the unstructured uncertainty can be useful for modelling the errors. There are several types of unstructured uncertainty models in literature, e.g. [30,31]:

- Additive Uncertainty
$$G(s) = \widetilde{G}(s) + W(s)\Delta(s). \tag{8}$$
- Multiplicative Uncertainty
$$G(s) = \widetilde{G}(s)(1 + W(s)\Delta(s)). \tag{9}$$
- Feedback Uncertainty
$$G(s) = \frac{\widetilde{G}(s)}{1 + W(s)\Delta(s)\widetilde{G}(s)}. \tag{10}$$
- Multiplicative Feedback Uncertainty
$$G(s) = \frac{\widetilde{G}(s)}{1 + W(s)\Delta(s)}. \tag{11}$$

In these models, $\widetilde{G}$ denotes the transfer function of the nominal plant, $W(s)$ is a proper and stable weight function representing uncertainty dynamics, and $\Delta(s)$ contains the uncertainty, which can be an arbitrary stable transfer function fulfilling the inequality:

$$\|\Delta\|_\infty \leq 1, \tag{12}$$

where

$$\|\Delta\|_\infty = \sup_{\omega \in \mathbb{R}} |\Delta(j\omega)| \tag{13}$$

is the norm of the Hardy space $\mathcal{H}_\infty$. The block diagrams of these uncertainty models are shown in Fig. 6.

Now, we want to describe the plant (1) with these uncertainty models using the identified interval uncertainty (2). With this extension we also cover nonlinearities such as hysteresis and other unmodelled dynamics. To do so, an appropriate weighting function W for each case should be found

Peer-reviewed version available at Algorithms 2020, 13, 24; doi:10.3390/a13010024

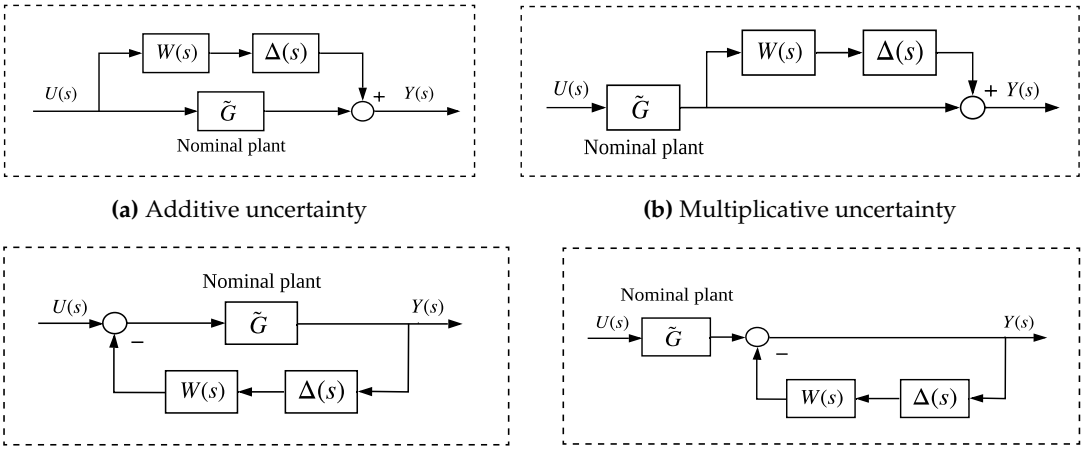

(a) Additive uncertainty

(b) Multiplicative uncertainty

(c) Feedback uncertainty

(d) Multiplicative feedback uncertainty

Figure 6. Uncertainty models of the plant's transfer function $G(s)$

such that condition (12) holds. First, we compute W for additive uncertainty case. Solving (8) for $W(s)\Delta(s)$ we get

$$W(s)\Delta(s) = G(s) - \widetilde{G}(s). \tag{14}$$

Together with the model's transfer functions (1) and (4) this results in

$$W(s)\Delta(s) = \frac{s(K\widetilde{T} - \widetilde{K}T) + K - \widetilde{K}}{s^2\widetilde{T}T + s(\widetilde{T} + T) + 1}.$$

A worst case scenario such that condition (12) is fulfilled can be obtained by replacing the unknown parameters K, T by their lower or upper bound as in (2), respectively. A possible solution fulfilling (12) is then given by

$$W(s) = \frac{s\left(\overline{K}\widetilde{T} - \widetilde{K}\underline{T}\right) + \overline{K} - \widetilde{K}}{s^2\widetilde{T}\underline{T} + s(\widetilde{T} + \underline{T}) + 1} \tag{15}$$

$$\Delta(s) = \frac{s^2\widetilde{T}\underline{T} + s(\widetilde{T} + \underline{T}) + 1}{s^2\widetilde{T}T + s(\widetilde{T} + T) + 1} \frac{s(K\widetilde{T} - \widetilde{K}T) + K - \widetilde{K}}{s(\overline{K}\widetilde{T} - \widetilde{K}\underline{T}) + \overline{K} - \widetilde{K}}. \tag{16}$$

Applying the same procedure to other uncertainty models, the weighting function W and the uncertainty function Δ can be described as follows:

- Multiplicative Uncertainty

$$W(s) = \frac{s\left(\overline{K}\widetilde{T} - \widetilde{K}\underline{T}\right) + \overline{K} - \widetilde{K}}{\widetilde{K}(s\underline{T} + 1)}, \quad \Delta(s) = \frac{s\underline{T} + 1}{sT + 1} \frac{s(K\widetilde{T} - \widetilde{K}T) + K - \widetilde{K}}{s(\overline{K}\widetilde{T} - \widetilde{K}\underline{T}) + \overline{K} - \widetilde{K}}. \tag{17}$$

- Feedback Uncertainty

$$W(s) = \frac{s\left(\overline{K}\widetilde{T} - \widetilde{K}\underline{T}\right) + \overline{K} - \widetilde{K}}{\underline{K}\widetilde{K}}, \quad \Delta(s) = \frac{\underline{K}}{K} \frac{s(K\widetilde{T} - \widetilde{K}T) + K - \widetilde{K}}{s(\overline{K}\widetilde{T} - \widetilde{K}\underline{T}) + \overline{K} - \widetilde{K}}. \tag{18}$$

- Multiplicative Feedback Uncertainty

$$W(s) = \frac{s(\widetilde{K}\overline{T} - \underline{K}\widetilde{T}) + \widetilde{K} - \underline{K}}{\underline{K}(1 + s\widetilde{T})}, \quad \Delta(s) = \frac{\underline{K}}{K} \frac{s(\widetilde{K}T - K\widetilde{T}) + \widetilde{K} - K}{s(\widetilde{K}\overline{T} - \underline{K}\widetilde{T}) + \widetilde{K} - \underline{K}}. \tag{19}$$

Peer-reviewed version available at Algorithms 2020, 13, 24; doi:10.3390/a13010024

Table 1. Robust stability conditions for different uncertainties [30,32]

Uncertainty type	Robust stability condition
$\widetilde{G} + W\Delta$	$\|WC\widetilde{S}\|_\infty < 1$
$\widetilde{G}(1 + W\Delta)$	$\|W\widetilde{T}\|_\infty < 1$
$\frac{\widetilde{G}}{1+W\Delta\widetilde{G}}$	$\|W\widetilde{G}\widetilde{S}\|_\infty < 1$
$\frac{\widetilde{G}}{1+W\Delta}$	$\|W\widetilde{S}\|_\infty < 1$

As mentioned before, the transfer functions W and Δ must be stable. In order to be stable, the transfer functions must also be proper, i.e., the degree of the numerator polynomial should not exceed the degree of the denominator polynomial. This structural condition is violated for the weighting function W of the feedback uncertainty model in (18). Therefore, this model it is not taken into account for robust controller design.

5.2. Robust Stability Analysis

Let $C(s)$ be a controller which stabilizes the nominal plant $\widetilde{G}(s)$ and $L(s)$ be the (nominal) open loop frequency transfer function, i.e.,

$$L(s) = C(s)\widetilde{G}(s). \tag{20}$$

Furthermore, let define $\widetilde{S}(s)$ and $\widetilde{T}(s)$ as the (nominal) sensitivity and complementary sensitivity function

$$\widetilde{S}(s) = \frac{1}{1 + L(s)} \quad \text{and} \quad \widetilde{T}(s) = \frac{L(s)}{1 + L(s)}. \tag{21}$$

Then, under assumption of additive uncertainty, the closed loop system with the plant (8) is robustly stable if and only if

$$\|WC\widetilde{S}\|_\infty < 1, \tag{22}$$

The inequality (22) can be adjusted into:

$$\left\| \frac{W(s)C(s)}{1 + C(s)\widetilde{G}(s)} \right\|_\infty < 1 \tag{23}$$

which means that that the envelope of Nyquist diagrams with radius $W(j\omega)\widetilde{G}(j\omega)$ and center $L(j\omega)$ cannot include the critical point $-1 \in \mathbb{C}$ due to the Small Gain Theorem.

The other uncertainties have different versions of such conditions. Table 1 summarizes the robust stability conditions for the uncertainty models.

5.3. Robust PI Control

A PI controller based on robust stability analysis is designed to investigate the effectiveness of the proposed method. The (nominal) open loop transfer function of the system is expressed as

$$L(s) = \left(K_p + \frac{K_i}{s}\right) \frac{\widetilde{K}}{1 + s\widetilde{T}}. \tag{24}$$

The (nominal) associated complementary sensitivity functions are given by

$$\widetilde{S}(s) = \frac{s(1 + s\widetilde{T})}{s^2\widetilde{T} + s(\widetilde{K}K_p + 1) + \widetilde{K}K_i}. \tag{25}$$

Peer-reviewed version available at Algorithms 2020, 13, 24; doi:10.3390/a13010024

$$\widetilde{T}(s) = \frac{\widetilde{K}(sK_p + K_i)}{s^2\widetilde{T} + s(\widetilde{K}K_p + 1) + \widetilde{K}K_i}. \tag{26}$$

By substituting the above equations in the the robust stability condition of each uncertainty model, the range of the proportional and integral gains for which the stability of the system is guaranteed can be obtained. To do so, the stability conditions of Table 1 are calculated and then plotted for different values of K_p and K_i as it is shown in Figures 7 and 8. Note that for our model the auxiliary transfer functions resulting from the additive and multiplicative model are the same. The level sets with values less than one fulfill the conditions and ensure robust stability.

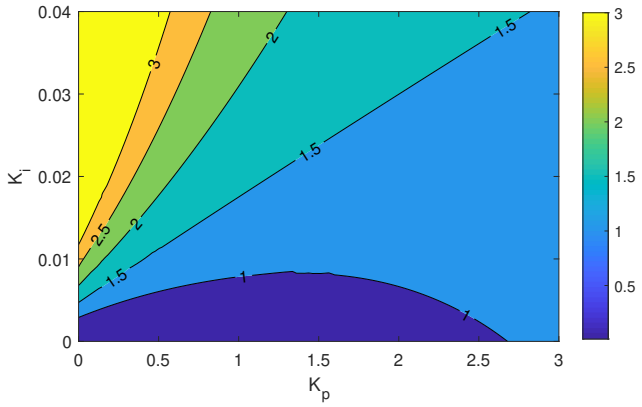

Figure 7. $\|WC\widetilde{S}\|_\infty$ and $\|W\widetilde{T}\|_\infty$ for different values of K_p and K_i for system with additive and multiplicative uncertainty respectively

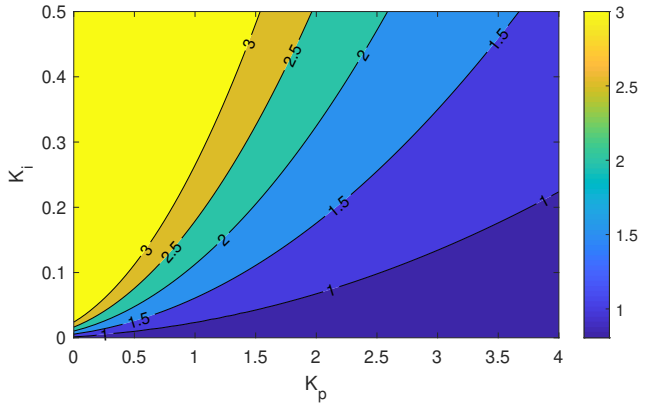

Figure 8. $\|W\widetilde{S}\|_\infty$ for different values of K_p and K_i for system with multiplicative feedback uncertainty

To verify the performance of the robust PI controller, output position control of the textile reinforced composite for a desired deflection is experimented. The selected gain values considering the additive/multiplicative uncertainty are $K_p = 2$ and $K_i = 0.004$. The Bode plot of the auxiliary transfer functions, $WC\widetilde{S}$ and $W\widetilde{T}$, is shown in Fig. 9. Clearly, the magnitude plot stays below $1 = 0_{\text{dB}}$ such that robust stability condition is fulfilled. The result of the experiment for a reference deflection of 22 mm is shown in Fig 10. It can be seen that the control action is really slow which is due to small value of the integral gain.

Peer-reviewed version available at Algorithms 2020, 13, 24; doi:10.3390/a13010024

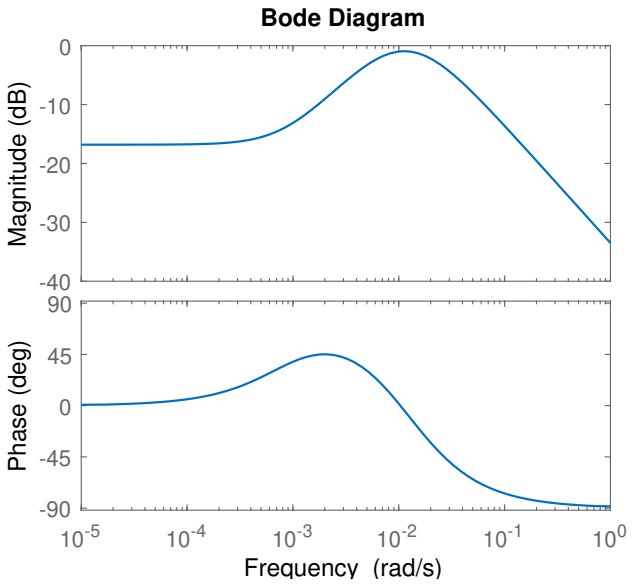

Figure 9. Bode plots of $W\widetilde{S}$ for $K_p = 2$ and $K_i = 0.004$ considering multiplicative uncertainty

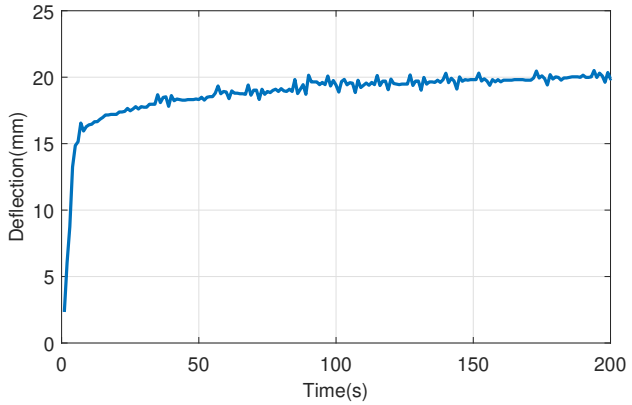

Figure 10. Controlled deflection of the system with multiplicative uncertainty for a reference of 22 mm using robust PI controller

The same experiment is repeated for the feedback multiplicative uncertainty case using the gain values $K_p = 3.2$ and $K_i = 0.16$. The Bode plot of the corresponding stability condition, $W\widetilde{S}$, using these gain values is shown in Fig. 11. Experimental result in Fig. 12 shows that this controller has a better performance with comparison to other uncertainty models and classical controller. It takes less time to reach the reference value. Furthermore, it provides stability for the whole set of plants described by (11).

Peer-reviewed version available at Algorithms 2020, 13, 24; doi:10.3390/a13010024

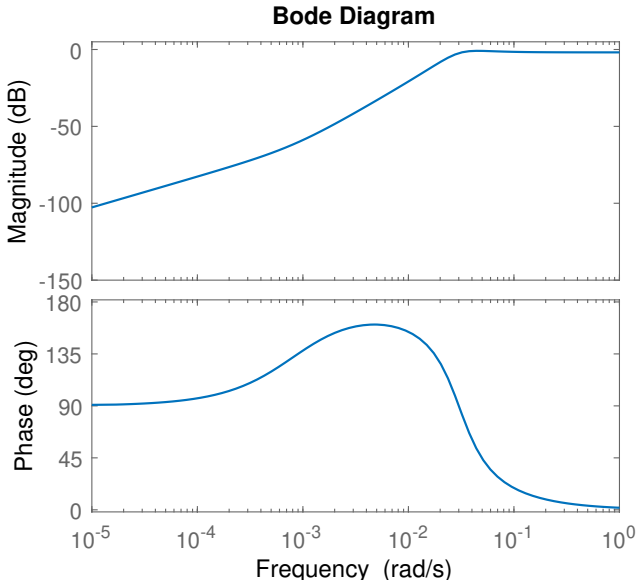

Figure 11. Bode plots of $W\widetilde{S}$ for $K_p = 3.2$ and $K_i = 0.16$ considering multiplicative feedback uncertainty

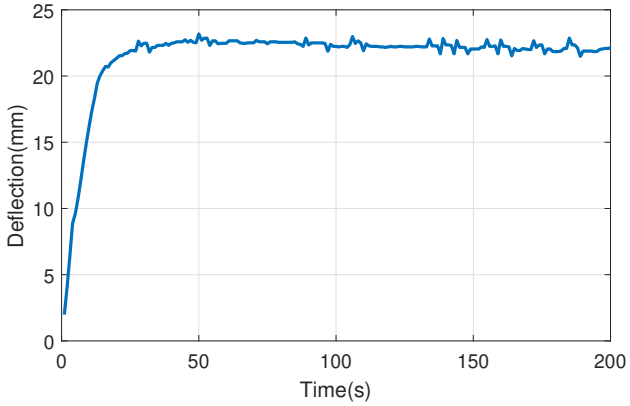

Figure 12. Controlled deflection of the system with multiplicative feedback uncertainty for a reference of 22 mm using robust PI controller

6. Conclusions

In this paper, the mathematical model of a textile reinforced composite actuated by shape memory alloys is described using various unstructured uncertainty models. Through this model the nonlinearities of the system including hysteresis are covered. The robust stability analysis of the proposed model is carried out and a robust proportional-integral controller based on this analysis is designed. Experimental results show the good performance of this controller in stabilizing the composite at a desired deflection.

Acknowledgments: The presented work was conducted for the project Research Training Group 2430 "Interactive Fiber Rubber Composites", which is funded by the Deutsche Forschungsgemeinschaft (DFG, German Research Foundation). The provided financial support is gratefully acknowledged. In addition, the authors would like to thank Dipl.-Ing. Klemens Fritzsche for interesting discussions which contributed to the paper.

References

1. Hughes, J.; Culha, U.; Giardina, F.; Guenther, F.; Rosendo, A.; Iida, F. Soft manipulators and grippers: a review. *Frontiers in Robotics and AI* **2016**, *3*, 69.

Peer-reviewed version available at Algorithms 2020, 13, 24; doi:10.3390/a13010024

2. Polygerinos, P.; Correll, N.; Morin, S.A.; Mosadegh, B.; Onal, C.D.; Petersen, K.; Cianchetti, M.; Tolley, M.T.; Shepherd, R.F. Soft robotics: Review of fluid-driven intrinsically soft devices; manufacturing, sensing, control, and applications in human-robot interaction. *Advanced Engineering Materials* **2017**, *19*, 1700016.
3. Rus, D.; Tolley, M.T. Design, fabrication and control of soft robots. *Nature* **2015**, *521*, 467–475.
4. Karaduman, N.S.; Karaduman, Y.; Ozdemir, H.; Ozdemir, G. Textile Reinforced Structural Composites for Advanced Applications. *Textiles for Advanced Applications* **2017**, p. 87.
5. Sohn, J.W.; Kim, G.W.; Choi, S.B. A state-of-the-art review on robots and medical devices using smart fluids and shape memory alloys. *Applied Sciences* **2018**, *8*, 1928.
6. Chopra, I. Review of state of art of smart structures and integrated systems. *AIAA journal* **2002**, *40*, 2145–2187.
7. Pelrine, R.; Sommer-Larsen, P.; Kornbluh, R.D.; Heydt, R.; Kofod, G.; Pei, Q.; Gravesen, P. Applications of dielectric elastomer actuators. Smart Structures and Materials 2001: Electroactive Polymer Actuators and Devices. International Society for Optics and Photonics, 2001, Vol. 4329, pp. 335–349.
8. Jin, M.; Lee, J.; Ahn, K.K. Continuous nonsingular terminal sliding-mode control of shape memory alloy actuators using time delay estimation. *IEEE/ASME Transactions on Mechatronics* **2014**, *20*, 899–909.
9. Suzuki, Y.; Kagawa, Y. Active vibration control of a flexible cantilever beam using shape memory alloy actuators. *Smart Materials and Structures* **2010**, *19*, 085014.
10. Dhanalakshmi, K.; Avinash, A.; Umapathy, M.; Marimuthu, M. Experimental study on vibration control of shape memory alloy actuated flexible beam. *International Journal on Smart Sensing & Intelligent Systems* **2010**, *3*.
11. Seelecke, S.; Mu¨ ller, I. Shape memory alloy actuators in smart structures: Modeling and simulation. *Appl. Mech. Rev.* **2004**, *57*, 23–46.
12. Sreekumar, M.; Nagarajan, T.; Singaperumal, M.; Zoppi, M.; Molfino, R. Critical review of current trends in shape memory alloy actuators for intelligent robots. *Industrial Robot: An International Journal* **2007**, *34*, 285–294.
13. Tanaka, K.; Nagaki, S. A thermomechanical description of materials with internal variables in the process of phase transitions. *Ingenieur-Archiv* **1982**, *51*, 287–299.
14. Liang, C.; Rogers, C.A. One-dimensional thermomechanical constitutive relations for shape memory materials. *Journal of intelligent material systems and structures* **1997**, *8*, 285–302.
15. Brinson, L.C. One-dimensional constitutive behavior of shape memory alloys: thermomechanical derivation with non-constant material functions and redefined martensite internal variable. *Journal of intelligent material systems and structures* **1993**, *4*, 229–242.
16. Mayergoyz, I.; Friedman, G. Generalized Preisach model of hysteresis. *IEEE transactions on Magnetics* **1988**, *24*, 212–217.
17. Brokate, M.; Sprekels, J. Hysteresis operators. In *Hysteresis and phase transitions*; Springer, 1996; pp. 22–121.
18. Al Janaideh, M.; Rakheja, S.; Su, C.Y. A generalized Prandtl–Ishlinskii model for characterizing the hysteresis and saturation nonlinearities of smart actuators. *Smart Materials and Structures* **2009**, *18*, 045001.
19. Ljung, L. Perspectives on system identification. *Annual Reviews in Control* **2010**, *34*, 1 – 12. doi:https://doi.org/10.1016/j.arcontrol.2009.12.001.
20. Isermann, R.; Münchhof, M. *Identification of Dynamic Systems – An Introduction with Applications*; Springer-Verlag: Berlin, Heidelberg, 2011.
21. Keshtkar, N.; Röbenack, K.; Fritzsche, K. Position Control of Textile-Reinforced Composites by Shape Memory Alloys. International Conference on System Theory, Control and Computing (ICSTCC 2019), Sinaia, Romania, 2019, pp. 442–447.
22. Cherif, C.; Hickmann, R.; Nocke, A.; Schäfer, M.; Röbenack, K.; Wießner, S.; Gerlach, G. Development and testing of controlled adaptive fiber-reinforced elastomer composites. *Textile Research Journal* **2018**, *88*, 345–353.
23. STMicroelectronics. *L298; Dual Full-Bridge Driver*, 2000. Datasheet.
24. Sharp. *GP2Y0A41SK0F, Distance Measuring Sensor Unit, Measuring distance: 4 to 30 cm, Analog output type*. Datasheet.
25. Röbenack, K. *Mobile Robotics with Arduino: Design and Programming*; CreateSpace Independent Publishing Platform, 2018.
26. Ljung, L. *System Identification Toolbox^{TM}*; The MathWorks, Inc.: Natick, MA, USA, 2012.

Peer-reviewed version available at Algorithms 2020, 13, 24; doi:10.3390/a13010024

27. O'Dwyer, A. *Handbook of PI and PID controller tuning rules*; Imperial College Press: London, 2009.
28. Datta, A.; Ho, M.T.; Bhattacharyya, S.P. *Structure and synthesis of PID controllers*; Springer-Verlag: London, 2000.
29. Franklin, G.F.; Powell, J.D.; Workman, M.L.; others. *Digital control of dynamic systems*, 3 ed.; Addison-Wesley: Menlo Park, CA, USA, 1998.
30. Zhou, K.; Doyle, J.C. *Essentials of Robust Control*; Prentice Hall: Upper Saddle River, New Jersey, 1998.
31. Matušů, R.; Prokop, R.; Pekař, L. Parametric and unstructured approach to uncertainty modelling and robust stability analysis. *International Journal of Mathematical Models and Methods in Applied Sciences* **2011**, *5*, 1011–1018.
32. Reinschke, K. *Lineare Regelungs- und Steuerungstheorie*, 2 ed.; Springer-Verlag: Berlin, Heidelberg, 2014.